Self-Interaction Corrected Density Functional Theory for the Study of Intramolecular Electron Transfer Dynamics in Radical Carbocations

Ivano Tavernelli

Laboratory of Computational Chemistry and Biochemistry, Ecole Polytechnique Fédérale de Lausanne, CH-1015 Lausanne, Switzerland

Received: August 21, 2007; In Final Form: October 9, 2007

We derived an orbital dependent Kohn−Sham based scheme for the correction of the self-interaction error in DFT, which is particularly suited for the study of open shell molecular systems. Our approach is based on a weighted form of the Perdew and Zunger (PZ) self-interaction correction scheme, in which an empirical coefficient is introduced in front of the SIC term to remove overcorrections. The method is used to investigate the first principle molecular dynamics of the intramolecular electron transfer (IET) in bis(methylene) adamanthyl radical cation and allows the analysis of the free energy surface that governs the IET process at room temperature (300 K). Indeed, the thermal activation of all molecular degrees of freedom provides important additional information about the mechanisms involved in the IET process. Our study confirms and extends previous results obtained with CASSCF and shows that there is no predominant degeneracy-lifting mode even at room temperature. However, we also identified regions in the phase space for which there is a significant probability for a productive IET event. In addition, we performed thermodynamic integrations along selected reaction coordinates to determine an estimate of the activation free energy barrier for the IET process.

1. Introduction

In KS-DFT the Coulomb interaction always contains a self-interaction term, because the cancellation between the Coulomb interaction energy of an electron in a given KS state with itself and the exchange−correlation term is generally incomplete. Even though most often neglected, the introduction of the self-interaction correction (SIC) to standard GGA functionals is required, especially in the case of charge transfer reactions involving open shell systems.

The standard scheme to approximately correct the self-interaction error (SIE) within GGA DFT implies the use of orbital-dependent Kohn−Sham potentials and was proposed by Perdew and Zunger (PZ).[1,2] This method requires the solution of unrestricted KS equations for each occupied KS state and leads, in general, to nonorthogonal KS orbitals, so that an *a posteriori* orthogonalization is required.[3] Even though the PZ-SIC significantly improves the energetics of a number of reaction barriers,[4] the scheme is computationally demanding and also reduces the accuracy of the calculations in the case where the effect of SIE is small, leading to poor geometries[5] and thermochemistry.[6]

Other schemes for the correction of SIE in DFT were proposed. In addition to the optimized potential method (OPM),[3,7−10] which apply naturally to the SIC problem due to its orbital dependent nature, a simplified SIC DFT scheme was recently proposed by d'Avezac, Calandra, and Mauri[11] and further discussed by VandeVondele and Sprik.[12] In these last two developments a correction is only applied to the frontier singly occupied KS orbital within a restricted open shell calculation. Because this orbital determines the spin density (SD) of the system, the correction is named SD-SIC. The method has a number of attractive features like the modest computational cost and the restriction of the correction to a single orbital, and was applied successfully to different systems with a single unpaired electron in the condensed phase[11,12] and molecules.[12]

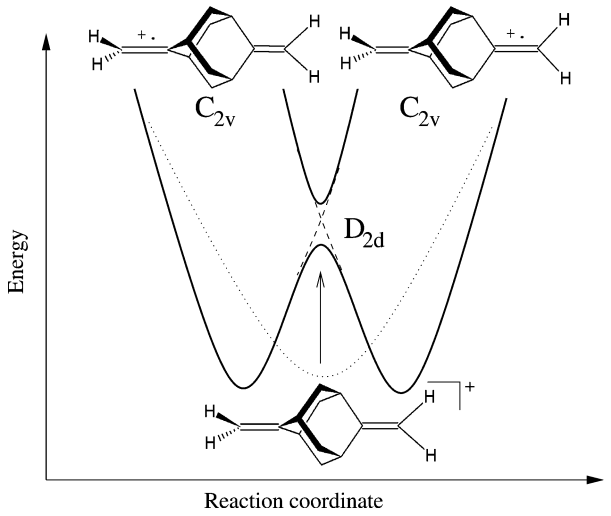

Figure 1. Schematic representation of the adiabatic potential energy surface for IET in BMA as a function of the antisymmetric stretch of the π-bonds. The structures with the corresponding localization (delocalization) of the positive charge are also shown for the two potential energy minima and the transition state. The dotted line represents the potential energy surface for BMA obtained using a standard GGA functional.

Unfortunately, the SD-SIC correction of Mauri was unable to reproduce the correct geometry for the optimized structure of many different radical carbocations. In particular, for the case of the model compound bis(methylene) adamantane radical (BMA), the localization of the unpaired electron on a single methylene π-bond could not be correctly reproduced (Figure 1). In this work, following the spirit of commonly used exact exchange corrected functionals, we use a weighted form of the PZ-SIC (wPZ-SIC) in which an empirical coefficient is intro-

10.1021/jp0767056 CCC: $37.00
Published on Web 12/01/2007

TABLE 1: Calibration of wPZ-SIC DFT[a]

system	spec.	bond	DFT	wPZ-SIC	ref
CH_3^+	D_{3h}	C−H	1.103	1.098/1.095/1.092	1.091[b]
$C_2H_4^+$	full rel.	C═C	1.426	1.398/1.39/1.375	1.405[c]
$C_3H_5^+$	full rel.	C−C	1.390	1.382/1.378/1.370	1.382[d]
		∠(C−C−C)	118.8	118.3/117.8/117.4	117.6[d]
BMA	C_{2v}	$(C═C)^0$		1.331/1.315/1.312	1.328[e]
		$(C═C)^+$		1.408/1.404/1.398	1.401[e]
	D_{2d}	C═C	1.375	1.369/1.361/1.357	1.366[e]

[a] Structural parameters for some organic carbon cations. wPZ-DFT values are compared with standard DFT data and reference values from other calculations and experiments. The three different values reported for wPZ-DFT correspond to weighting factors $w_{SIC} = 0.25$,0.35, and 0.45, respectively. The structure with C_{2v} symmetry corresponds to the absolute energy minima. The two π-bonds have different lengths, the hole being localized on the methylene unit, $(C═C)^+$. Within standard DFT no charge localization is observed. The D_{2d} structure is associated with a charge-delocalized cation radical. Distances are given in Å and angles in degrees. [b] Data from ref 38. [c] Data from ref 39. [d] Data from ref 40. [e] Data from ref 20.

duced in front of the PZ-SIC term to compensate for the overcorrection in PZ-SIC DFT. The additional parameter is then optimized to reproduce correct geometries in a training set composed by simple organic radical cation compounds (Table 1).

In the traditional picture of Marcus theory, charge transfer processes are described by the mixing of two diabatic states, one representing the electronic configuration with the charge localized on the donor site, and the other one representing the configuration of the product state with the charge on the acceptor moiety. In the region where the two surfaces approach each other, the eventual mixing between them can give rise to an avoided crossing. In such an adiabatic picture, the coupling splits the two potential energy surfaces (PESs), the ground state and the first excited state, by an amount equal to the double of the coupling. In the weak coupling limit the donor and acceptor diabatic states are characterized by well defined and distinguished electronic configurations, and the electron transfer (ET) rate is simply given by the *Fermi Golden Rule*,[13,14]

$$k_{ET} = \frac{1}{\hbar}|T_{DA}|^2 \, FC \tag{1}$$

where T_{DA} is the effective ET matrix element and FC is the Franck−Condon factor. For many cases Marcus theory[15−17] provides a valid approximation for FC

$$FC = \sqrt{\frac{\pi}{k_B T E_\lambda}} e^{-\Delta G^{\ddagger}/k_B T} \tag{2}$$

where E_λ is the reorganization free energy and $\Delta G^{\ddagger}$ is the activation free energy.

The knowledge of the correct reaction coordinate that drives the system from the donor to the acceptor state is therefore crucial for the determination of the rate. Along this path, the value of the electronic coupling and the probability to reach the avoided crossing can then be computed, together with the transfer rate, according to eq 1.

In this work we address the problem of the determination of the free energy surfaces that govern intramolecular electron transfer (IET) in the model compound BMA at room temperature. The process involves an electron transfer between the π-bonds connected by the adamantane spacer (AD) and is characterized at zero temperature by a vanishingly small coupling due to the different symmetries of the orbitals of the donor and acceptor states.

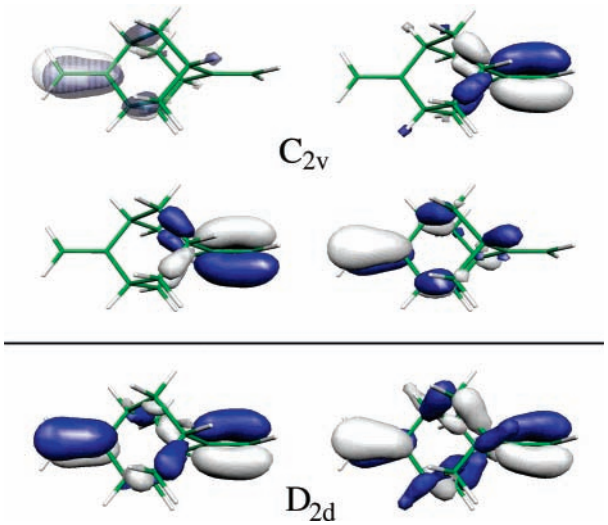

Figure 2. Frontier orbitals of BMA at different molecular symmetries represented by an envelope of constant amplitude (± 0.05 Å$^{-3/2}$). In the upper panel the singly occupied HOMO−1 and HOMO Kohn−Sham orbitals are shown for the α (left) and β (right) spins. In the D_{2d} symmetry both singly occupied HOMO KS orbitals are delocalized on both π-systems.

Using the implemented wPZ-SIC DFT based MD approach at room temperature, we observe a thermally induced breaking of the molecular D_{2d} symmetry at the surface crossing, which was at the origin of the *diabatic trapping* mechanism discussed in ref 18. In this picture, the minimum free energy reaction path for the IET cannot be simply described in terms of the gradient difference (GD) and nonadiabatic coupling (DC) vectors that split the ground state/excited state energy degeneracy at the conical intersection at zero Kelvin. Temperature activates additional internal degrees of freedom, which in turn modify substantially the topology of the free energy surface governing the IET process.

2. Ground State IET vs Diabatic Trapping

Previous computational studies have addressed the problem of identifying the important vibrational modes that are responsible for the removal of the symmetry constraints that reduce the coupling matrix elements to zero. In the case of the molecule BMA in its D_{2d} configuration the electronic coupling for the IET should in principle be very small. Nevertheless, rapid IET is observed at rates greater than 10^8 s^{-1}.[19] Using a semiempirical trajectory surface hopping approach, Jones et al.[20] could show that molecular vibrations can open the energy gap between ground-state and first excited-state adiabatic PESs even in the case of potentially symmetry forbidden IET processes. The same system was also the subject of the work by the groups of Paddon-Row[20,21] and Robb,[18,22] in the last case using an ab initio approach based on CASSCF. Their aim was to identify the condition for the so-called diabatic trapping in BMA studying the PES in the microcanonical ensemble. They were able to identify the two coordinates that, in first-order perturbation, lift the degeneracy at the intersection of the two adiabatic states. The first branching-state coordinate consists of the antisymmetric stretching (AS) of the two π-bonds, which brings the system close to the crossing point (or seam) between the two surfaces, whereas the coordinate that causes the splitting is an antisymmetric breathing mode of the BMA skeleton (the adamantane bridge unit). According to their analysis of the PES, the adiabatic trapping in BMA occurs because the length of the branching space vector associated to this vibrational mode is small.

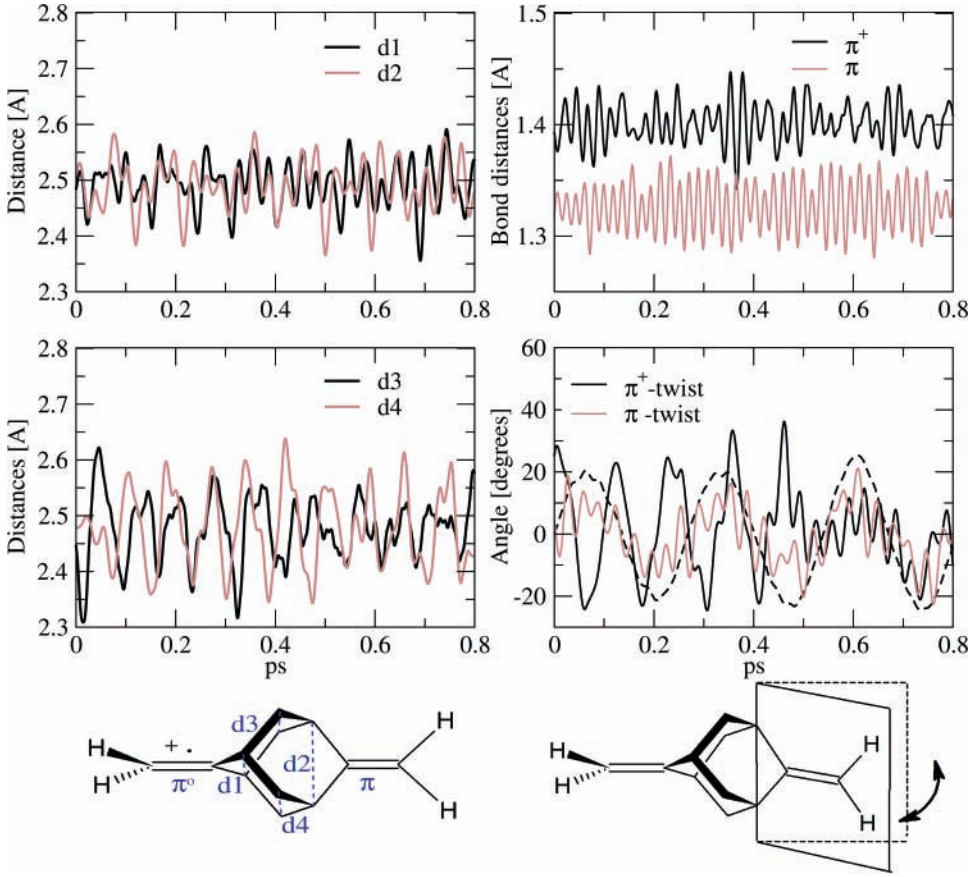

Figure 3. Time series for some relevant intramolecular distances computed from the unconstrained MD trajectory at 300 K (for the definition of the distances see the molecule sketch on the left). Left column: intramolecular distances within the adamantane structure. Right column: in the upper panel we report the time series for the vibration of the π-bonds. The π^+-bond is in average 0.075 Å longer than the other, as was the case for the optimized structure. In the lower panel we have monitored the out-of-plane twisting of the π-bonds around their planar structure (same color code as in the upper panel). The broken line refers to the oscillation of one methylene unit as a whole around its optimized position (see the molecule sketch on the right).

Here we extend the calculation of the IET process in BMA to the canonical ensemble (NVT) and study the implications of temperature in the activation of nonharmonic modes, which cannot be observed by performing a zero-temperature vibrational analysis.

3. Methods

3.1. SIC Corrected DFT. As mentioned in the Introduction, we employ a SIC corrected DFT scheme for which the standard KS-DFT equations are augmented with a weighted PZ-SIC term.

The minimization of the wPZ-SIC KS equations

$$(\mathscr{H}_0^\sigma + w_{\mathrm{SIC}} V_i^{\mathrm{SIC},\sigma})\phi_i^\sigma = \epsilon_i^\sigma \phi_i^\sigma + \sum_{j\neq i}^{\mathrm{occ}} \lambda_{i,j}\phi_j^\sigma \qquad (3)$$

is carried on under the constraint that the orbitals ϕ_i^σ ($\sigma = \alpha, \beta$) be orthonormal

$$\langle \phi_i^\sigma | \phi_j^\sigma \rangle = \delta_{i,j} \qquad (4)$$

In eq 3, $\mathscr{H}_0^\sigma$ is the standard KS Hamiltonian

$$\mathscr{H}_0^\sigma = -\frac{1}{2}\nabla^2 + V_{\mathrm{H}}^\sigma[n] + V_{\mathrm{ext}}^\sigma[n] + V_{\mathrm{xc}}^{\mathrm{GGA},\sigma}[n^\alpha, n^\beta] \qquad (5)$$

with

$$V_{\mathrm{H}}^\sigma[n] = \int \frac{n^\sigma(r')}{|r-r'|}\,\mathrm{d}r' \qquad (6)$$

$$V_{\mathrm{xc}}^{\mathrm{GGA},\sigma}[n^\alpha, n^\beta] = \frac{\delta E_{\mathrm{xc}}^{\mathrm{GGA}}[n^\alpha, n^\beta]}{\delta n^\sigma(r)} \qquad (7)$$

$V_i^{\mathrm{SIC},\sigma}$ is the orbital dependent SIC correction term

$$V_i^{\mathrm{SIC},\sigma} = -\int \frac{n_i^\sigma(r')}{|r-r'|}\,\mathrm{d}r' - V_{\mathrm{xc}}^{\mathrm{GGA},\sigma}[n_i^\sigma, 0] \qquad (8)$$

$\lambda_{i,j}$ are the Lagrangian multipliers to impose orthogonality, and w_{SIC} is a parameter that is derived from calibration studies on a training set of molecules.

At each MD step the SIC energy is minimized by the conjugated gradient method. Due to the orbital dependence of the potential $V_i^{\mathrm{SIC},\sigma}$, the optimization does not preserve orthonormality, and therefore, it is necessary to orthogonalize the orbitals at each step. In addition, the energy of the system can be further lowered by the mixing of all KS wavefunctions according to a unitary transformation. This follows from the fact the SIC correction is not invariant under such operation. Summarizing, the optimization procedure consists of three operations: (1) minimization step, (2) unitary mixing of the orbitals, and (3) orthogonalization. In this work, we replace step (2) by a orbital localization procedure based on maximally localized Wannier functions.[23]

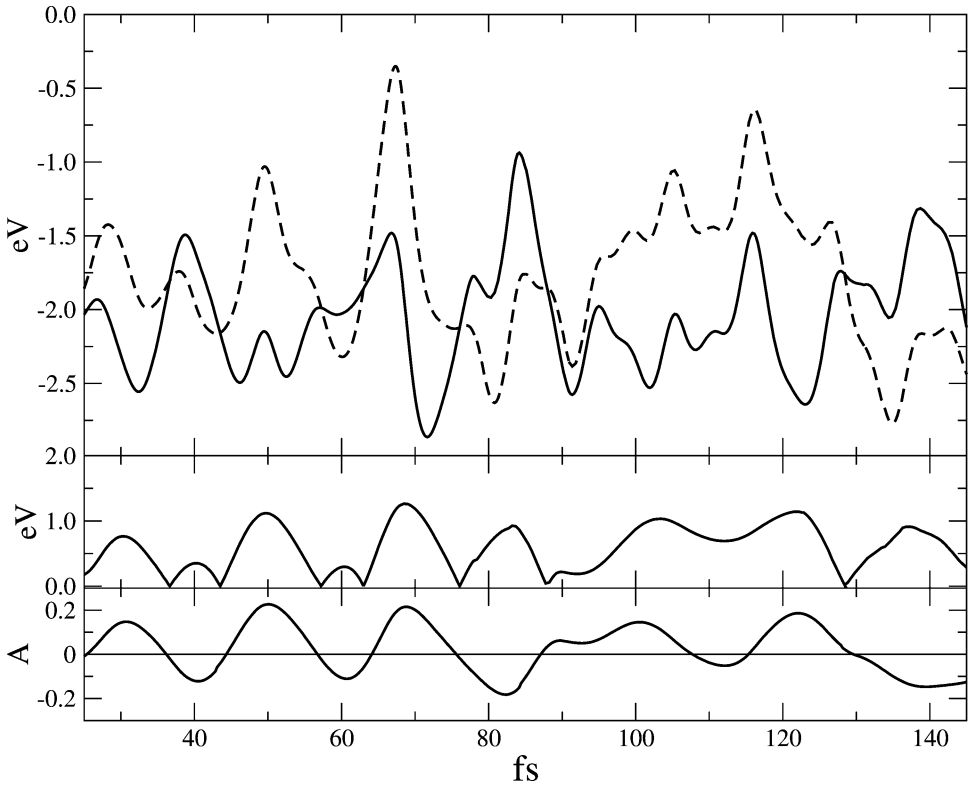

Figure 4. Time series of the two PESs (in eV) corresponding to the different localization of the unpaired electron (upper panel). The dynamics is computed at 300 K using an external potential applied to the methylene units to keep the system close to the seam of intersections (see text). The forces for the dynamics are computed from the PES shown in a continuous line. The middle panel shows the time series of the energy gap (in eV), and the lower panel reports the time series of the bond length difference (in Å) between the two π-bonds.

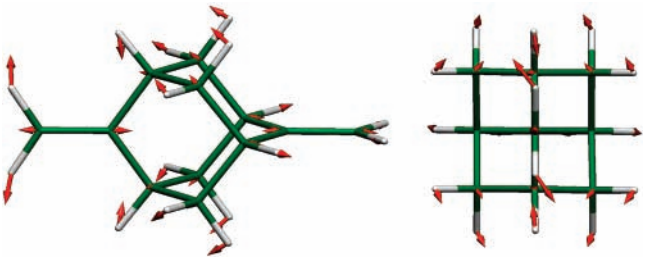

Figure 5. Two different views of the atomic structure and velocities for the trajectory frame corresponding to time 93 fs in Figure 4. The methylene group bearing the positive charge is on the left side (lateral view) and shows a fast rotation of both hydrogen atoms along the C−C axes.

3.2. Thermodynamic Integration. The present work aims at the study the effects of temperature in governing the mechanism of IET between the two methylene units in BMA. For this purpose, we use a thermodynamic integration scheme for the calculation of the free energy profile along the reaction coordinates given by the bond length of one ethylene unit (R_π or R_{π^+}) or the following linear combination of the two

$$\Delta R_{\pi,\pi^+} = (\lambda - 1)R_\pi + (1 - \lambda)R_{\pi^+} \qquad \lambda \in [0, 1] \qquad (9)$$

Here and in the following we label with the π^+ double bond carrying the positive charge (hole) and with π the uncharged one.

We performed molecular dynamics calculations for different values of the π-bond lengths, ranging from 1.315 to 1.405 Å, where the two extremes correspond to the π- π^+-bond lengths, respectively.

The distance constraint during the MD simulation was maintained via a Lagrangian multiplier, λ, and the free energy profile was then constructed from

$$\Delta F(R) = -\int_{R_{\min}}^{R_{\max}} \mathrm{d}R' \, \langle\lambda\rangle_{R'}^{\mathrm{cond}} - F_0 \qquad (10)$$

where $\Delta F(R)$ denotes the relative free energy as a function of the bond length and F_0 is a constant reference free energy. $\langle\lambda\rangle_{R'}^{\mathrm{cond}}$ is a conditional ensemble average of the Lagrange multiplier with reaction coordinate fixed at value R'

$$\langle\lambda\rangle_{R'}^{\mathrm{cond}} = \frac{\int \mathrm{d}^N p \, \mathrm{d}^N r \, \lambda(p,r) \mathrm{e}^{-\beta H(p,r)} \delta(R - R')}{\int \mathrm{d}^N p \, \mathrm{d}^N r \, \mathrm{e}^{-\beta H(p,r)} \delta(R - R')} \qquad (11)$$

where p and r denote the collective momenta and coordinates of the system, $H(p,r)$ is the N-particle Hamiltonian, and $\beta = 1/k_B T$. In practice, the ensemble averages are evaluated as weighted averages over the constrained MD trajectories. The error in the thermodynamic integration is analyzed according to ref 24. For all 4 ps long trajectories computed at different constraints, the Lagrange multipliers λ were sampled at every time step (0.24 fs). The corresponding mean forces $\langle\lambda\rangle$ were then calculated, along with their standard deviations σ_λ. Finally, the standard deviations in the mean, $\sigma_{\langle\lambda\rangle}$, were estimated by taking into account the statistical dependency of the sampled points.[24] The statistical errors associated with the calculation of the free energy profile are determined by accumulating the error over the integration in eq 10 using standard error propagation rules.

The computed potential at mean force acting on the constraint corresponds to the free energy difference between the starting configuration (with no constraint) and the constrained ones.

Apart from the constraints on the π-bond lengths, all other molecular degrees of freedom are free to move and therefore are sampled according to their Boltzmann weights at the chosen temperature. In this way, we obtained an unbiased description of the additional conformational changes involved in the IET process.

As we will explain in more detail below, in addition to the zero temperature vibrational motions carefully described in,[18,22] we observed global conformational changes induced by temperature, which influence the free energy reaction barrier and the switch among the diabatic states.

3.3. Computational Details. wPZ-SIC MD calculations are carried out with the plane wave code CPMD.[25] The PBE[26] functional is employed. We use soft norm-conserving nonlocal Troullier−Martins pseudopotentials[27] and a 60 Ry energy cutoff for the plane wave expansion of the wavefunction. All energies and gradients are converged to a maximum deviation of 10^{-7} au. All MD simulations have been performed in the NVT ensemble using a isolated cell of $15 \times 10 \times 10$ Å^3 and a time integration step of 10 au (0.24 fs). A Nosé−Hoover thermostat[28−30] was used to control the system temperature. In the computation of the free energy profile we performed a series of constrained MD simulations at 300 K for different values of the constrained methylene bond length ranging from 1.315 to 1.405 Å in steps of 0.01 Å.

wPZ-SIC calculations are computationally quite demanding because of the orbital dependence of PZ-SIC term, which is applied to all KS orbitals. A wavefunction optimization requires on average ∼20 SCF iterations to reach convergence, each iteration being 5−6 times slower than the one required in a standard GGA-DFT calculation.

4. Results and Discussion

4.1. SIC Calibration. The results of the calibration process used to determine the weighting coefficient w_{SIC} in the wPZ-SIC functional are shown in Table 1. The training set is composed of simple carbon cations CH_3^+, the ethylene cation $C_2H_4^+$, the allyl cation $C_3H_5^+$, the unsaturated ethylene radical cation, and BMA. For all these systems, high-level calculations and experimental determined geometrical parameters are available for comparison. As a whole, we observe a net increase in the performance of PBE-DFT when the SIC correction is switched on. All bond lengths and angles systematically improve and approaches the reference values for w_{SIC} in the range 0.25−0.45. Further increase of the weighting coefficient w_{SIC} beyond this values induces an overcorrection in the self-interaction term and all covalent bonds become too short.

In general, the correction becomes important when charge separation is also taking place (like in BMA). In the case of unsaturated cations, like ethylene and BMA in the C_{2v} symmetry, we do not observe the out-of-plane twist of ∼22° of the π-system suggested by some experimental and computational studies.[20] This point should be clarified by future higher-level calculations, but because we are interested in finite-temperature properties the exact nature of the optimize structure should not affect our calculations. In addition, room-temperature trajectories clearly show an activation of the twisting motion of the π-bonds in BMA (see Figure 3).

Throughout this work we fix the value of the SIC coefficient to $w_{SIC} = 0.35$.

4.2. Ground State Potential Energy Surface. At the GGA-DFT level of theory the ground state global minimum energy structure for the BMA radical cation has a D_{2d} symmetry and the positive charge is formally delocalized on both methylene units. This simple calculation clearly shows the limits of standard DFT in reproducing the correct C_{2v} global energy minimum already known from CI and CASSF calculations.[18] However, using the proposed wPZ-SIC DFT scheme with a weighting factor $w_{SIC} = 0.35$, we can reproduce with good accuracy the high-level ab initio data. The correct minimal energy structure shows two inequivalent π-bond systems, in which the positive charge is mainly localized on one of the two methylene groups (π^+ double bond). Consequently, the two double bonds have unequal lengths of 1.404 and 1.315 Å, respectively, which compare well with the AM1-CI data, 1.401 and 1.328 Å.[20] As in the case of ref 18, we do not observe any twist of the π-bonds away from the C_{2v} conformation, in contrast to what previously suggested from AM1-CI calculations.[20] On the other hand, a twist of the π^+-bond is indeed observed during the MD simulation carried out at room temperature.

Along the reaction coordinate given by the AS of the double bonds the system reaches a seam of intersections[18,22] for a geometry with D_{2d} symmetry and with the hole delocalized on the two double bonds. This configuration is Jahn−Teller unstable and relaxation along the same asymmetric π-bond stretching causes the system to relax back into one of the two equivalent global energy minima with consequent charge localization. The magnitude of the nonadiabatic coupling at the seam is very small (less than $K_BT \simeq 0.026$ eV at 300 K) and suggests therefore a purely nonadiabatic mechanism for the associated intramolecular ET process. As a consequence, no charge transfer is expected along the AS coordinate until the system reaches the transition state (seam of intersection), where the charge is eventually transferred "instantaneously" from one π-bond to the other. The quality of the computed potential energy surface along the AS is in agreement with previous calculations: the energy difference between the global minimum and the TS is 3.07 kcal/mol at wPZ-DFT, 3.1 kcal/mol at AM1-CI, and 3.36 kcal/mol at CASSCF level of theory.

The relevant wPZ-SIC KS frontier orbitals of BMA are displayed in Figure 2 for both C_{2v} and D_{2d} symmetries. In the perfectly symmetric D_{2d} geometry the nonadiabatic coupling between the two diabatic PESs is zero and the ET process is symmetry-forbidden. We therefore conclude that thermal fluctuations may induce a partial reduction of the adamantane D_{2d} symmetry element at the seam, and the symmetry braking will only be complete at the PES minima.

4.3. Molecular Dynamics. Blancafort et al. discuss the occurrence of diabatic trapping using a microcanonical on-the-fly semiclassical dynamical approach.[31] They conclude that in BMA there is no single mode that controls the alternative between ET and diabatic trapping at the seam of intersections. On the contrary, the size of the energy gap between GS and excited state energy surfaces appears to be a result of the combination of different collective modes. According to their results, the second branching space coordinate at the seam (the GD coordinate) described by the "antisymmetric breathing" of the rigid adamantane frame, and the torsion of the terminal methylene units[20,21] are not the only ones involved in the mechanism of diadatic trapping in BMA. The present work aims to investigate the nature of the additional degrees of freedom that play an important role in lifting of the adiabatic trapping in BMA at room temperature and that cannot be captured by the microcanonical MD technique used in ref.[18]

In Figure 3 we show the time series of the thermally induced vibrations of a selected set of relevant degrees of freedom. The simulation was carried out at a temperature of 300 K and for a total length of 2 ps. The first row in Figure 3 reports the time

series for four interatomic distances measured within the adamantane unit, showing the amplitude of the "breathing" motion associated to the rigid structure of the bridge. The oscillations have similar frequencies and they tend to run in phase confirming the collective character of the breathing mode. The 300 K vibrational frequency of the two π-bonds is shown in the top right panel. The average length of the cation π^+ double bond (black line) is about 0.075 Å longer than the normal π-bond, but the oscillation frequencies are similar (ω_π being 1.25 larger than ω_{π^+}). Interestingly, we observe collective vibrational modes involving the methylene moieties as a whole (Figure 3 lower right panel, broken line). This vibration was not observed in previous MD studies[20,22,18] because it gets activated only when the temperature is raised above about 50 K. In addition, the out-of-plane torsion of the two methylene groups is also observed during the dynamics at room temperature. Figure 3 (lower right panel) shows the time series for the plane twist of the two π-bonds. The maximal rotation in the case of the π^+ double bond is 30°, which is very close to the values measured experimentally. The twist of the uncharged π-system is instead strongly modulated by the out-of-plane displacement of the methylene unit (broken line), and the high-frequency component has a much smaller amplitude.

Because of the size of the activation barrier for the IET in BMA, it is very unlikely to observe a spontaneous charge transfer event in BMA by means of unbiased room-temperature MD trajectories. To gain insights about the dynamics of the electron transfer process, we enriched the sampling of the configuration close to the transition state by means of a biased MD simulation where both π-bonds are restrained around a distance of 1.36 Å by a harmonic potential with a force constant of 0.05 au. This trajectory of a total length of 1 ps shows several PES crossings. Figure 4 reports the time series of the PES driving the dynamics ($\pi-$AD$-\pi^+$, continuous line) together with the one corresponding to the other diabatic state (π^+-AD$-\pi$, broken line). Because the energy gap at the crossing is generally very small (<0.01 eV), the system is kept always on the same diabatic state for the full length of the simulation. The calculation of the potential energy for the electron transfer state was obtained by constraining the density optimization algorithm to converge toward the local energy minimum with the inverted localization of the hole and corresponding positive charge.

Along the trajectory, the time derivative of the PES difference at the avoided crossings is on average quite large (in absolute value) and the energy gap between the two PESs rather small (a fraction of kcal/mol). According to Landau−Zener (LZ) theory,[32,33] this translates into a very low probability for an exchange of diabatic state. Therefore the system is mainly subject to diabatic trapping. On the other hand, in few cases—as, for example, in the time interval 88−98 fs—the two surfaces run in parallel for an appreciable amount of time. This leads to a coupling of the two PESs with a consequent transfer of amplitude according to the surface hopping (SH) scheme description of nonadiabatic transitions.[34] LZ SH probabilities at the energy gap minima between the adiabatic PESs are computed using the approach described in refs 35 and 36. In Figure 4, at the minimum time 93 fs, the probability for a surface hop reduces to 73%. Statistically, this means that for particular geometries sampled during the MD there is an appreciable probability for a productive IET, which takes the system from one diabatic state to the other. We have identified several other events similar to the one just described, all giving IET probabilities between 10% and 35%. The trajectory frame (atomic position and velocities) at the point of maximal probability is shown in Figure 5. As expected, this structure has similar bond lengths for both methylene units, but instead of an AS we observe a synchronous elongation of both π-bonds. The principal dynamical mode associated with this part of the trajectory is characterized by the rotation of the two hydrogen atoms of the π^+-unit along the C−C axis.

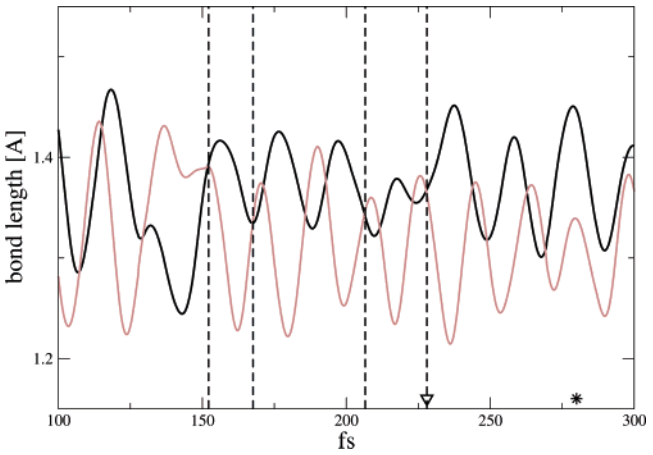

Figure 6. Time series of the π-bond lengths measured along the 300 K trajectory with harmonic restrains as in Figure 4. The vertical broken lines indicate the points of intersection between the two surfaces. These occur at geometries with similar methylene bond lengths. The star indicates the starting point for the unconstrained trajectories, which are used to monitor the relaxation of the system into the two equivalent global free energy minima.

In Figure 6 we report the time series of the π- and π^+-bond lengths in a time window that shows four sequential surface crossings (vertical dotted lines). The surface crossings occur at geometries with equally long π-bonds. However, for these structures R_π ($=R_{\pi^+}$) usually differs from the average bond length $\langle R_\pi \rangle = 1.36$ Å computed as the average of the room-temperature mean values for R_π and R_{π^+}. This observation suggests that the region of contact between the ground and first excited state (seam of intersections) extends for a wide region of the free energy surface, but with the restriction of the two π-bonds having the same length.

Figure 7 shows the structure of BMA at the surface crossing indicated with a triangle in Figure 6. The geometry is almost perfectly linear, with equally long π-bonds and a twist of the positively charged methylene units of about 21.5°.

To follow the relaxation dynamics from the seam of intersection to the free energy minima, we selected a geometry close to the surface crossing (from the trajectory obtained with the harmonic bias potential, see asterisk in Figure 6) and we ran a new trajectory according to the unconstrained potential in eq 3. To avoid an excessive transfer of kinetic energy to the ionic degrees of freedom, we coupled the system with a Nosé−Hoover thermostat at 300 K.

It is interesting to observe that the relaxation of the system back to the minimum of the free energy surface does not occur in a simple monotonic descent as suggested by the one-dimensional energy plot in Figure 1. Instead, the room-temperature free energy hypersurface close to the crossing region between the two diabatic states shows a much richer structure (Figure 8, upper panel). The trajectory remains trapped in the crossing region for about 0.2 ps and eventually undergoes subsequent recrossings before finding the way toward the free energy minima. The probability for an IET event computed with the LZ scheme is negligibly small at all crossings. The energy fluctuations at the beginning of the simulation are initially quite important (bigger than the energy difference between the top

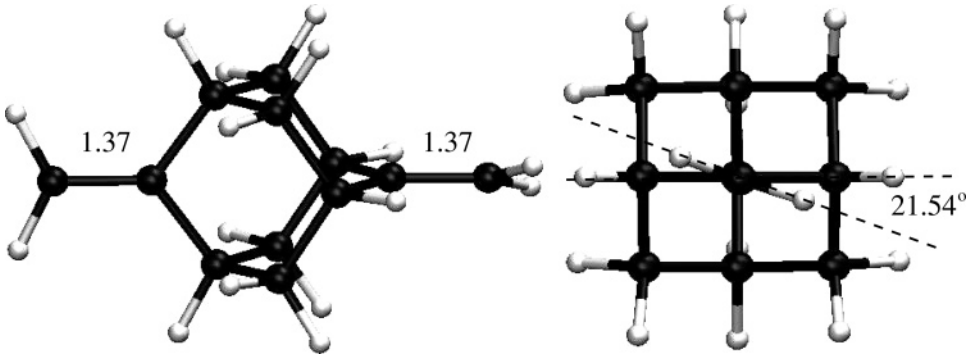

Figure 7. BMA structure at the point of vanishing energy gap (frame labeled with a triangle in Figure 6). The π-bonds have the same length. A twist of one methylene unit of about 21.5° is also observed.

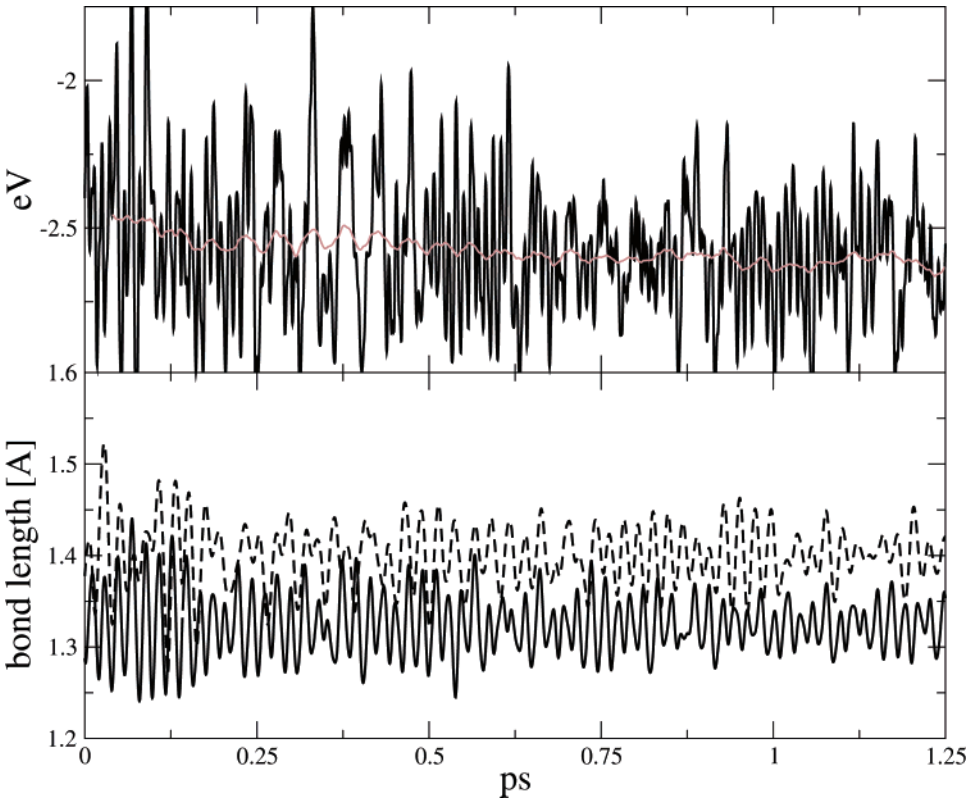

Figure 8. Time series of the total energy (upper panel) and of the π-bonds bond lengths (lower panel) computed along an unconstrained 300 K trajectory started from a frame labeled with a star in Figure 6. The brown line in the upper panel corresponds to a running average over 500 points of the black curve. The system remains for about 0.25 ps near the region of intersection between the two PESs, before relaxing toward one of the global free energy minima. The first part of the dynamics is characterized by large fluctuations of the π-bonds.

of the barrier and the energy minimum), but they become smaller as the system relaxes into the PES minima because of the dissipation of the excess energy into the coupled reservoir. We can also use this trajectory to characterize the structural and dynamical features that distinguish the regions of the phase space close to the seam of intersection from the one at the minima. During the first part of the trajectory, the two double bonds oscillate in phase (symmetric stretch), which corresponds to a motion perpendicular to the main reaction coordinate (AS) for the IET (Figure 1). This concerted motion is, however, unstable and after less than 200 fs the two vibrational modes go out of phase as a consequence of the redistribution of the kinetic energy. Once the hole gets stabilized on one side of the molecule we observe a clear separation of the two vibrational modes. The positively charged double bond elongates and oscillates with a frequency about 0.85 times the one of the neutral double bound.

For a characterization of the structures close to the seam of intersections, the difference between the π- and π^+-bond lengths is not the only quantity of interest. At sufficiently high temperatures (room temperature), thermal oscillations are enough to bring occasionally the system in configurations with $\Delta R_{\pi\pi^+} = 0$ (see lower panel in Figure 8), which, however, are characterized by an energy gap with the first excited state bigger than 1 eV and, therefore, lie very far from the region of surface crossings. We have identified two additional global variables that show a clearly different behavior during the first and the last part of the relaxation trajectory. They correspond to the distances d_1 to d_4 introduced in Figure 3. In Figure 9 we show the time series of these distances computed during the restrained dynamics (harmonic potentials on the double bonds), during the free relaxation dynamics (after removal of the harmonic restraining potential), and at equilibrium. When the system is forced to move perpendicular to the reaction coordinate

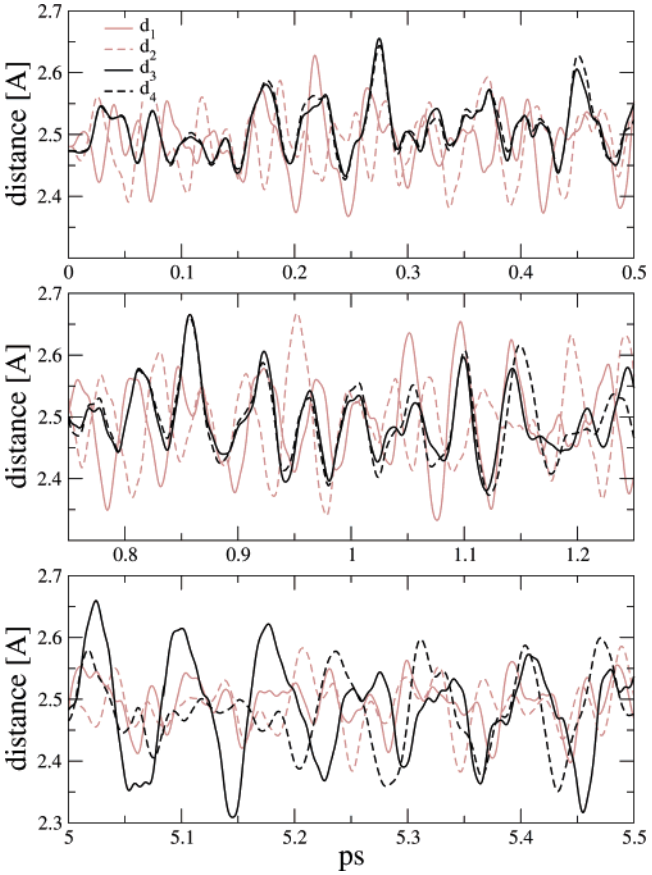

Figure 9. Time series of the intramolecular distances d_1 to d_4 as defined in Figure 3 measured for three different time windows of 0.5 ps each along the relaxation dynamics in Figure 8.

(constrained run), the d_3 and d_4 distances are very similar at all times, but they gradually lose correlation during the relaxation along the unconstrained PES (middle panel). The thermalized run at 300 K confirms this trend and shows a clear loss of correlation among the four distances (Figure 9, lower panel).

4.4. Thermodynamic Integration. According to the Fermi Golden Rule, eq 1, the rate for IET transfer depends crucially from the coupling matrix element, T_{DA}, and the activation free energy barrier $\Delta G^{\ddagger}$. As already mentioned above, the relatively small kinetic constant associated to this process implies very long simulation times, which are beyond the affordable time scales of modern ab initio MD simulations. To compute the free energy profile for the room-temperature IET process in BMA, we therefore applied a thermodynamic integration scheme along selected reaction coordinates. In the case of BMA the choice of the reaction coordinate is quite straightforward and coincide with the "derivative coupling" coordinate used in refs 18 and 22, which consists of the simultaneous stretching and shortening of the π- and π^+-bonds, respectively.

To perform the thermodynamic integration, we used two different reaction coordinates based on the antisymmetric stretching of the two π-bonds. In the first setup we computed the work done on the system during the independent stretching of the π-bond from 1.32 to 1.36 Å and shrinking of the π^+-bond from its equilibrium value of 1.401 to 1.36 Å. The total work needed to bring the system to the conical intersection was then computed as the sum of the two independent contributions. In the second setup, we computed the collective work along the collective reaction coordinate $\Delta R_{\pi,\pi^+}$ in eq 9, which assumes a simultaneous antisymmetric stretch of both π-bonds. It is important to stress that the remaining nuclear degrees of freedom

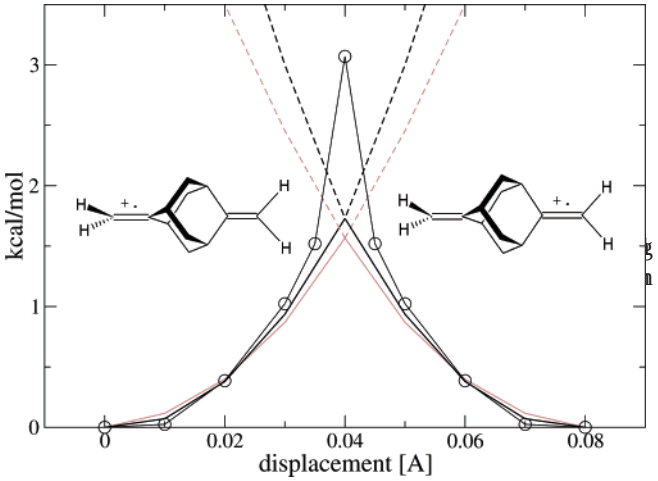

Figure 10. Energy and free energy profiles along the antisymmetric stretch of the π-bonds. The black curves are computed using the combined reaction coordinate, $\Delta R_{\pi\pi^+}$, defined in eq 9. The free energy profile is obtained using a thermodynamic integration scheme at 300 K, and the energy curve (symbols) refers to geometry optimized structures. In brown we show the free energy profile obtained from the sum of the work contributions computed for the independent stretches of the two π-bonds along the reaction coordinate $\Delta R_{\pi} = R_{\pi}^0 - R_{\pi}$ and $\Delta R_{\pi^+} = R_{\pi^+}^0 - R_{\pi^+}$, respectively (where R_{π}^0 and $R_{\pi^+}^0$ represent the 300 K equilibrium bond lengths). The nature of the diabatic states is showed schematically in the insets. The broken lines show the evolution of the free energy surfaces in the case there would be no IET.

The results of the two simulations are reported in Figure 10, together with the 0 K energy profile connecting the structures of C_{2v} and D_{2d} symmetry. We first observe that both reaction coordinates, namely the combination of ΔR_{π} and ΔR_{π^+}, and the collective coordinate $\Delta R_{\pi,\pi^+}$, give very similar free energy profiles. The free energy barrier, $\Delta G^{\ddagger}$ computed by thermodynamic integration is about 1.5 ± 0.4 kcal mol^{-1} lower than the energy difference measured along the antisymmetric collinear stretch of the π-bonds. The entropy contribution at room temperature favored therefore the configurations close to the region of intersections. This observation is also confirmed by the larger amplitude of the π-bond oscillations measured during the first ~0.2 ps simulation of the unconstrained trajectories in Figure 8.

5. Conclusions

Self-interaction corrected DFT within the GGA approximation offers the possibility to extend the applicability of DFT to the study of radical carbocations and, possibly, to other molecular and condensed phase systems in which electron localization plays a major role. Because of its simple physical interpretation and its relatively easy implementation, a number of studies on SIC corrected DFT have already been performed, showing the validity of this correction in different contexts.[37]

In this study, we have reported the implementation of a "weighted" Perdew−Zunger SIC scheme for the GGA approximation to the exchange−correlation energy. The presence of a weighting factor, w_{SIC}, in front of the PZ correction is justified by the incomplete cancellation of the self-interaction error in standard GGA functionals. The optimal value for w_{SIC} was found to be 0.35. The optimization of this parameter for all carbocations in the training set shows a weak dependence of the energy and of all monitored geometrical parameters on the value of w_{SIC} within ~0.2 and ~0.5. In the specific case of the BMA molecule, all geometrical parameters are in good agreement with the CASSCF data available in the literature.[22]

The method was combined with a first principle molecular dynamics scheme for the study of the IET process in BMA at room temperature. This approach allows for an efficient sampling of the configurational space according to the corresponding Bolzamann weights, and therefore allows the investigation of the thermally activated modes that may control the IET rate. By means of a restrained dynamics approach we have enriched the region of the phase space in the neighborhood of the avoided crossing (seam of interactions) with the aim to study the dynamics of the IET process.

Temperature has several effects in determining the reaction rate for the IET process in BMA. First, the thermal activation of additional degrees of freedom contributes to lower the free energy barrier for the IET. Second, the same modes also influence the way the two diabatic states are crossing. In agreement with the CASSCF and AM1-CI studies, virtually no charge transfer is detected until the molecule reaches the transition state characterized by equally long methylene bonds. However, we found crossings between the two PESs for a wide range of values of $R_\pi = R_{\pi^+}$ between 1.34 and 1.38 Å. At the point of crossing, rotation of the plane containing the methylene hydrogen atoms was also observed. In addition, at low temperature the crossing along the ANTI occurs sharply, but at finite temperature we observe different topologies of the surface crossing region (Figure 4). Of particular interest is the case in which the two PESs run in parallel for several fs in the region of strong coupling. This induces a finite transition probability from one diabatic state to the other and promotes therefore the ET process. Finally, the structural distortions associated to the different ground state energy minima induce a memory in the electronic structure of the molecules, which is responsible for a phenomena that we may call *dynamic trapping*. When crossing the seam of intersections, the systems keeps information about the structure associated to the past diabatic state, and even though a surface switch may occur, the system tends to stay in, or return to, the PES corresponding to the original electronic configuration. Although the first two phenomena have the effect of increasing the ET rate, the third one increases the probability for a back-transfer into the original state, decreasing therefore the number of effective IET events.

Acknowledgment. The author thanks U. Rothlisberger and M. Cascella for fruitful discussions.

References and Notes

(1) Perdew, J. P.; Zunger, A. *Phys. Rev. B* **1981**, *23*, 5048.
(2) Patchkoskii, S.; Ziegler, T. *J. Phys. Chem. A* **2002**, *106*, 1088.
(3) Lindgren, I. *Int. J. Quantum Chem. Symp.* **1971**, *5*, 411.
(4) Patchkoskii, S.; Ziegler, T. *J. Chem. Phys.* **2002**, *116*, 7806.
(5) Goedecker, S.; Umrigar, C. J. *Phys. Rev. A* **1997**, *55*, 1765.
(6) Vydrov, O. A.; Scuseria, G. E. *J. Chem. Phys.* **2004**, *121*, 8187.
(7) Norman, M. R.; Koelling, D. D. *Phys. Rev. B* **1984**, *30*, 5530.
(8) Harrison, J. G. *J. Chem. Phys.* **1983**, *78*, 4562.
(9) Harrison, J. G. *J. Chem. Phys.* **1983**, *79*, 2265.
(10) Harrison, J. G. *J. Chem. Phys.* **1987**, *86*, 2849.
(11) d'Avezac, M.; Calandra, M.; Mauri, F. *Phys. Rev. B* **2005**, *71*, 205210.
(12) VandeVondele, J.; Sprik, M. *Phys. Chem. Chem. Phys.* **2005**, *7*, 1363−1367.
(13) Marcus, R. A.; Sutin, N. *Biochim. Biophys. Acta* **1984**, *811*, 256.
(14) Mikkelsen, K. V.; Ratner, M. A. *Chem. Rev.* **1987**, *87*, 113.
(15) Marcus, R. A. *J. Chem. Phys.* **1956**, *24*, 966−978.
(16) Marcus, R. A. *J. Chem. Phys.* **1956**, *24*, 979−989.
(17) Marcus, R. A. *Annu. Rev. Phys. Chem.* **1964**, *15*, 155.
(18) Blancafort, L.; Hunt, P.; Robb, M. *J. Am. Chem. Soc.* **2005**, *127*, 3391−3399.
(19) De Cola, L.; Balzani, V.; Barigelletti, F.; Flamigni, L.; Belser, P.; Bernhard, S. *Recl. trav. Chim. Pays-Bas* **1995**, *114*, 534−541.
(20) Jones, G. A.; Carpenter, K.; Paddon-Row, M. N. *J. Am. Chem. Soc.* **1999**, *121*, 11171−11178.
(21) Jones, G. A.; Paddon-Row, M. N.; Carpenter, B. K.; Piotrowiak, P. *J. Phys. Chem. A* **2002**, *106*, 5011−5021.
(22) Blancafort, L.; Jolibois, F.; Olivucci, M.; Robb, M. *J. Am. Chem. Soc.* **2001**, *123*, 722−732.
(23) Marzari, N.; Vanderbilt, D. *Phys. Rev. B* **1997**, *56*, 12847.
(24) Allen, M. P.; Tildesley, D. J. *Computer Simulation of Liquids*; Oxford University Press: New York, 1987.
(25) *CPMD;* Copyright IBM Corp 1990−2001, Copyright MPI fuer Festkoerperforschung Stuttgart, 1997−2001; http://www.cpmd.org.
(26) Perdew, J. P.; Burke, K.; Ernzerhof, M. *Phys. Rev. Lett.* **1996**, *77*, 3865.
(27) Troullier, N.; Martins, J. L. *Phys. Rev. B* **1991**, *43*, 1993.
(28) Nosé, S. *J. Chem. Phys.* **1984**, *81*, 511−519.
(29) Nosé, S. *Mol. Phys.* **1984**, *52*, 255−268.
(30) Hoover, W. G. *Phys. Rev. A* **1985**, *31*, 1695−1697.
(31) Herman, M. F. *Ann. Rev. Phys. Chem.* **1994**, *45*, 83−111.
(32) Landau, L. D. *Phys. Z. Sowjetunion* **1932**, *2*, 46.
(33) Zener, C. *Proc. R. Soc. London Ser. A* **1932**, *137*, 696.
(34) Tully, J. C.; Preston, R. K. *J. Chem. Phys.* **1971**, *55*, 562.
(35) Jones, G. A.; Carpenter, K.; Paddon-Row, M. N. *J. Am. Chem. Soc.* **1999**, *120*, 5499−5508.
(36) Mercier, S. R.; Boyarkin, O. V.; Kamariotis, A.; Guglielmi, M.; Tavernelli, I.; Cascella, M.; Rothlisberger, U.; Rizzo, T. R. *J. Am. Chem. Soc.* **2006**, *128*, 16938−16943.
(37) Cascella, M.; Cuendet, M. A.; Tavernelli, I.; Rothlisberger, U. *J. Phys. Chem. B* **2007**, *111*, 10248−10252.
(38) Kapp, J.; Screiner, P. R.; Schleyer, P. v. R. *J. Am. Chem. Soc.* **1996**, *118*, 12154−12158.
(39) Köppel, H.; Domcke, W.; Cederbaum, L. S.; von Niessen, W. *J. Chem. Phys.* **1978**, *69*, 4252.
(40) Reidl, B.; Clark, T.; Schleyer, P. v. R. *J. Comput. Chem.* **1997**, *18*, 533−551.